Molecular determinants for effective siRNA protection and transfection mediated by cyclooligosaccharide-based nanoparticles.

D. Manzanares[1,2], I. Araya-Durán[3], L. Gallego-Yerga[4], P. Játiva[1,2], V. Márquez-Miranda[3], J. Canan[3], J. L. Jiménez Blanco[4], C. Ortiz Mellet[4], F. Danilo González-Nilo[3,5,6]J. M. García Fernández[7] and V. Ceña[1,2,*]

[1] Unidad Asociada Neurodeath, Universidad de Castilla-La Mancha, Albacete, Spain; [2]CIBERNED, Instituto de Salud Carlos III, Madrid. Spain; [3]Universidad Andres Bello, Facultad de Ciencias Biológicas, Center for Bioinformatics and Integrative Biology (CBIB), Av. República 239, Santiago, Chile, 8370146; [4]Departamento de Química Orgánica, Facultad de Química, Universidad de Sevilla, C/ Profesor García González 1, 41012-Sevilla Sevilla, Spain; [5]Fundación Fraunhofer Chile Research, Las Condes, Chile,7550296; [6] Centro Interdisciplinario de Neurociencia de Valparaíso, Facultad de Ciencias, Universidad de Valparaíso, Valparaíso, Chile, 2360102; [7]Instituto de Investigaciones Químicas (IIQ), CSIC - Universidad de Sevilla, Vda. Américo Vespucio 49, 41092 Sevilla, Spain.

***** Address correspondence to:

Prof. Valentín Ceña
Universidad de Castilla-La Mancha
Unidad Asociada Neurodeath
Facultad de Medicina
Avda. Almansa, 14
02006 Albacete (SPAIN)
Email: valentin.cena@gmail.com
Telephone +34 680222322

Abstract

Aim: In this study, the siRNA complexing properties and transfection capabilities of two pairs of cyclooligosaccharide-based molecular nanoparticles, namely polycationic amphiphilic cyclotrehalan and cyclodextrin derivatives, were evaluated and the structural requirements that govern their efficiency as nonviral vectors investigated by in silico modelling.

Materials and Methods: The stability of the cyclooligosaccharide/siRNA nanocomplexes and their endosome escape capabilities were studied by agarose gel electrophoresis and fluorescence techniques; the thermodynamic parameters of the nanoparticle/siRNA interactions were calculated by molecular dynamics simulations and the data were related with the siRNA transfection efficiencies in cellulo.

Results: The lower the siRNA solvent accessible surface area in the presence of the molecular nanoparticle, the higher the protection from RNAse-mediated degradation in the corresponding nanocomplex; a moderate molecular nanoparticle/siRNA binding energy value further facilitates siRNA release and binding to the target mRNA upon cell uptake.

Conclusions: The use, in advance, of these parameters will provide a useful indication of the potential of a molecular nanoparticle as siRNA transfecting vector.

Keywords: siRNA transfection, endosomal escape, protein knock down, molecular modeling, protection from RNAses, molecular nanoparticle

Introduction

The use of interference RNA (RNAi) technology provides a very effective gene silencing mechanism that represents an innovative approach to study the role of certain proteins in the physiology or pathology of different organs by knocking down the protein of interest and studying the behaviour of the system in the absence of such a protein [1]. It represents a good alternative to knock-out mice since it does not generate compensatory pathways during development, it is faster and it can be used even with proteins whose removal is lethal at embryonic stages [2]. Moreover, RNAi has been proposed to be useful in therapeutics since it is able to knockdown proteins involved in the pathogenesis of different diseases by targeting their mRNA [3]. In addition, RNAi-mediated knockdown of proteins involved in cancer cell survival has been proposed to potentiate antitumoral actions of drugs [4], establishing another potential therapeutic approach for cancer treatment.

RNAi operates in most eukaryotic cells [5],[6] and comprises duplex RNA sequences of 21-23 base pairs that directly inhibit homologous genes. Under physiological conditions, it regulates the activity of microRNAs (miRNAs) that are involved in the regulation of key cellular functions like cell differentiation, metabolism or malignant transformation [7]. MicroRNAs regulate cellular functions by forming staggered RNA duplexes of 21-24 base pairs that are directed to the target mRNA to specifically knock-down the encoded protein. Several exogenous activators of the RNAi system can silence specific sequences involved in cellular signalling, being small interfering RNAs (siRNAs) the most widely used. siRNAs are double-strand RNAs each one formed by about 21 nucleotides that degrade homologous mRNAs [8]. They are

highly effective for protein knockdown, but they are quickly degraded in the extracellular medium and they do not enter the cell in naked form, requiring the use of carriers (vectors) to protect them from degradation and to transport them to the cell interior [9].

Different types of nanoparticles (NPs) have been used to efficiently transfect siRNA into different cell types [1][10], and whole animals [11]. To produce an efficient transfection, the NPs, together with the siRNA cargo, must circumvent several barriers. First, it should interact with the siRNA, generally by electrostatic interactions involving positive charges located at the NP periphery [12]. The nanoparticles should be also able to protect the siRNA from degradation by RNAses present in the culture medium or in plasma [10]. Nanoparticle/siRNA complexes must then be taken up by the cells through mechanisms that generally involve endocytosis, either through clathrin or caveolae-dependent routes [13], allowing them to enter the endosome/lysosome pathway [14]. Lysosomes contain a significant number of hydrolytic enzymes that can degrade a broad range of NPs and their attached cargos, including DNA, RNA, many proteins and therapeutic agents. For this reason, endosomal escape is one of the major limiting steps for the efficiency of NPs to deliver functional siRNA to different cell types that would be able to knockdown the target protein [15].

As mentioned above, to be efficient transfection vectors, NPs should have positive charges on its surface to bind the negatively charged siRNA [12]. Depending on the nature of the cationizable groups, the NPs can also contribute to facilitate the endosomal escape. For instance, highly positively charged siRNA carriers based in either poly(ethylenimine) (PEI) or PAMAM dendrimers, which are very efficient at

transfecting various cell lines [16], possess buffering capabilities and are assumed to benefit from the so-called “proton-sponge” mechanism. Briefly, protonation of some of the amino groups in these vectors occurs at the endosomal acidic pH, causing chloride anion and water entry, osmotic swelling and vacuole disruption, ultimately leading to release of the NPs and their cargo to the cell cytosol [17]. Unfortunately, the enhanced transfection effect of highly positively charged vectors is achieved at the cost of high toxicity that severely limits their biomedical applications [14].

So far, there is no clear understanding of the characteristics that a chemical entity must fulfill to successfully complete the above pathway leading to efficient siRNA delivery that might help to predict the NP transfection behavior. Consequently, the development of most siRNA transfection vectors has been based on trial and error approaches. The development of high-precision methodologies for accessing well-defined molecular architectures of nanometric dimensions (molecular NPs) offers unique possibilities to change this scenario [18]. Macrocyclic platforms, among which macrocyclic carbohydrate derivatives are paradigmatic examples, have shown to be particularly well-suited for strategies directed to generate structural diversity in molecular NPs with nucleic acid delivery capabilities [19]. In addition to their biocompatible character, cyclooligosaccharide carriers can be subjected to systematic structural modifications, while keeping diastereomeric purity [20]. We took advantage of these properties to get information on the molecular determinants underlying the efficient complexation and delivery of siRNA by synthesizing two pairs of positively charged amphiphilic molecules built on face-differentiated cyclooligosaccharide scaffolds with very similar topologies. The first pair, namely

compounds EMA5 and EMA6, comprises a central convex-type macroring formed by two α,α'-trehalose disaccharide moieties linked through their primary positions by thiourea groups (cyclotrehalans) [21] and feature segregated polycationic (6 or 18 protonable nitrogens, respectively) and hydrophobic (6 myristoyl chains) domains. The second pair, namely compounds AMC6 and AMC36, share a basket-shaped β-cyclodextrin core [22] with 7 oligoethylenimine branches at the primary (narrower) rim containing either 28 (AMC6) or 35 protonable nitrogens (AMC36) and 14 hexanoyl chains at the opposite secondary face (Figure 1). In all cases, electrostatic interactions between the molecular vectors and siRNA are supposed to lead to the formation of nanoparticle/siRNA complexes. Non-amphiphilic cyclodextrin derivatives bearing similar cationic heads had been reported to mediate transfection is some cell lines [Srinivasachari S, Fichter KM, Reineke TM: Polycationic β-cyclodextrin "click clusters": monodisperse and versatile scaffolds for nucleic acid delivery, J. Am. Chem. Soc. 130, 4618-4627 (2008)]. Yet, on selecting the vector candidates for this study we keep in mind that several studies have later shown that amphiphilicity significantly improves the nucleic acid complexing capabilities and the transfection efficiency of the corresponding self-assembled nanoparticles [Jiménez Blanco JL, Benito JM, Ortiz Mellet C, García Fernández JM: Molecular nanoparticle-based gene delivery systems. J. Drug Deliv. Sci. Technol. DOI: 10.1016/j.jddst.2017.03.012 (2017)].

Data revealed, however, striking differences in the capabilities of the different molecular NPs included in this study to protect siRNA from degradation by RNAses present in the environment and/or in their transfection properties. Thus,

cyclotrehalan EMA5 does not protect the siRNA cargo from RNAse-mediated degradation while its homologue EMA6 does. On the other hand, β-cyclodextrin AMC6 is very efficient at transfecting siRNA while AMC36, which differs only in having one extra amino group in each oligoethylenimine branch, does not have any transfection ability. We have used *in silico* modelling to identify the molecular determinants of such a behavior and found that the smaller the value for the siRNA solvent accessible surface area (SASA) in the presence of the molecular NP, the higher the probability of being protected from RNAse-mediated degradation. On the other hand, a high energy binding between the molecular NP and siRNA inhibits the dissociation of the later from the nanocomplex so precluding it from binding to the target mRNA and, accordingly, from knocking down the target protein.

Material and Methods

General methods

Optical rotations were measured at 20 ± 2 °C in 1-dm tubes on a Jasco P-2000 polarimeter. Ultraviolet-visible (UV) spectra were recorded in 1-cm tubes on a Beckman DU640 UV spectrophotometer. Infrared (IR) spectra were recorded on a Jasco FT/IR 6000-Series spectrophotometer. ^{1}H (and ^{13}C NMR) spectra were recorded at 300 (75.5), 500 (125.7) MHz with Bruker 300 AMX, 500 AMX and 500 DRX. 1D TOCSY, 2D COSY, HMQC and HSQC experiments were used to assist on NMR assignments. Thin-layer chromatography (TLC) was carried out on aluminium sheets coated with Kieselgel 60 F254 (E. Merck), with visualization by UV light and by charring with 10% H_2SO_4. Column chromatography was carried out on Silica Gel 60 (E. Merck, 230-400 mesh) for preparative purposes. ESI mass spectra were recorded in the positive mode on an Esquire 3000 ion-trap mass spectrometer (Bruker Daltonik GmbH). Elemental analyses were performed at the Instituto de Investigaciones Químicas (Sevilla, Spain) using an elemental analyser Leco CHNS-932 or Leco TryuSpec CHN. Heptakis(6-azido-6-deoxy-2,3-di-*O*-hexanoyl)cyclomaltoheptaose **(1)** [23], N^1,N^2,N^3,N^4,N^5-{tetraethylenepenta[(*tert*-butoxycarbonyl)amino]}ethylene-N^6-propynamide (**2**) [24], 6,6'-dideoxy-6,6'-diiodo-α,α'-trehalose (**4**) [25], 6,6'-dideoxy-2,3,4,2',3',4'-hexa-*O*-(3-(2-*N*-*tert*-butoxycarbonylaminoethylthio)-propyl)-6,6'-diisothiocyanato-α,α'-trehalose (**8**) [26], 2-[bis[2-(*tert*-butoxycarbonylamino)ethyl]amino]ethyl isothiocyanate (**10**) [27], and compound **AMC6** were prepared according to reported procedures [28].

Synthesis of new compounds.

A detailed account of the synthesis and characterization of the new compounds can be found in the Supporting Information section.

Agarose gel retardation

Agarose gel electrophoresis was performed as previously described [29]. Nanoparticle/siRNA complexes were prepared at pH 5.5 using 100 nM siRNA and increasing nanoparticle concentrations to achieve the desired N/P ratios. The mixture was incubated for 30 min at room temperature. Samples were loaded onto 1.2% agarose gel containing ethidium bromide (50 µg/mL). Electrophoresis was carried on at 60 mV for 15 min, and the resulting gels were photographed under UV-illumination. The fluorescent bands were acquired and digitized using a developer (Vilber, Marne-la-Vallée, France) and analysed using the Image J program [30]

siRNA protection against RNAses

The cyclooligosaccharide-based molecular nanoparticles were incubated for 30 minutes with siRNA at the N/P ratio of 6.67 for AMC6; 4.17 for AMC36; 4.29 for EMA5; and 4.28 for EMA6, corresponding to a siRNA:NP 1:10 molar ratio, which provided full retention of siRNA (100 nM) in the gel retardation experiments. Then, RNAse (0.25% w/v; Sigma, Barcelona; Spain) was added and incubated for 30 min at 37 ºC. RNAse was then inactivated by cooling the samples at 4 ºC for 15 min and heparin (0.5 USP units) was added for an additional 20 min period at 4 ºC to completely release siRNA from the NP while RNAse remained inactivated as previously described [4]. Samples were then loaded onto a 1.2% agarose gel

containing ethidium bromide (50 µg/mL), and run under the same experimental conditions as indicated above. Fluorescent bands were acquired and digitized using a developer (Vilber, Marne-la-Vallée, France) and analysed using the Image J program [30]

Cell culture

The rat glioblastoma C6 cell line was obtained from ATCC (Manassas, VA, USA). The cells were grown in Dulbecco's Modified Eagle's Medium (DMEM) supplemented with 10% heat-inactivated foetal calf serum; 2 mM L-glutamine, 5 µg/mL streptomycin and 20 units/mL penicillin. Cells were maintained at 37 ºC in a humidified atmosphere containing 5% CO_2.

Endosomal escape assay

Endosomal escape was studied as previously described [31] with some modifications. Briefly, C6 cells were plated on 20 mm diameter glass coverslips at 33,000 cells/mL and cultured for 48 hours. Cells were washed 3 times using Krebs-Henseleit (K-H) solution with the following ionic composition (in mM): NaCl, 140; $CaCl_2$, 2.5; $MgCl_2$, 1; KCl, 5; Hepes 5 mM, Glucose, 11; pH was adjusted to 7.4. Cells were then incubated in Opti-MEM medium containing 250 µM calcein (Sigma-Aldrich, Barcelona, Spain) alone or together with the indicated molecular NP (1 µM) for 4 hours. At that time, the Opti-MEM containing calcein or calcein plus the NP was removed, the coverslip washed twice with DMEM to remove non- taken up NPs or calcein and the cells incubated in DMEM supplemented with 10% heat-inactivated foetal calf serum; 2 mM L-glutamine, 5 µg/mL streptomycin and 20 units/mL penicillin. Cells were maintained at 37 ºC in a humidified atmosphere containing 5%

CO_2 until its use. Ten minutes before recording, Hoescht 33342 (25 µg/mL) (ThermoFisher, Waltham, Massachusetts, USA) was added to label the nuclei. At the indicated times, cells were washed 3 times with K-H solution and mounted on the stage of a Nikon Eclipse TE2000-E fluorescence microscope (Nikkon, Tokyo, Japan) and fluorescence recorded using 60x fluorescence oil immersion objectives. Excitation wavelengths were 350 nm for Hoechst 33342 and 470 nm for calcein and the emission wavelengths were 450 nm for Hoechst 33342 and 509 nm for calcein. Data were acquired using NIS Elements AR software (Nikkon, Tokyo, Japan).

siRNA transfection and Western blot analysis

Cells were incubated with the cyclooligosaccharide-based molecular nanoparticles alone or with nanoparticles/siRNA nanocomplexes formed by incubating the corresponding NP (1 µM) with either scramble siRNA or specific siRNA (100 nM; Sigma, Barcelona, Spain) for rat p42-Microtubule-associated protein kinase (p42-MAPK; sense: 5'-GUAUAUACAUUCAGCUAAUAU-3', antisense: 5'-AUAUUAGCUGAAUGUAUAUAC-3') for 30 minutes. When Interferin® (Polyplus, Illkirch, France) was used, as reference transfection method, to form complexes with siRNA, manufacturer instructions were followed. Cells were treated for 72 hours, the medium was washed twice and the cells lysed. Western blots were performed as previously described using 15 % PAGE-SDS gels [32]. The following antibodies were used: polyclonal anti-p42-MAPK antibody (1:1000) (Cell Signaling Techology, Beverly, MA, USA) and polyclonal anti-β-actin antibody (1:4000) (Sigma Chemical Co., St. Louis, MO, USA) to correct for protein loading. Immunocomplexes were visualized using an enhanced chemiluminiscence system (Millipore, Bedford, MA,

USA). Densitometric analysis of immunoreactive bands was performed using the Image J program [30].

Molecular dynamics simulations

Two sets of molecules, namely the cyclotrehalan derivatives EMA5 and EMA6 and the β-cyclodetrin derivatives AMC6/AMC36, were modeled in this study. For this purpose, the full atom structure of each molecule was split up into three components. Three monomers (TAI, COR and TER) were built (Figure 2) following our previous published approach [33] and then parameterized using the online platform PARAMCHEM and the CHARMM General force field (CGenff) [34],[35]. Parameters for the carbohydrates that belong to the ring (COR) of the molecules were obtained from the force field CHARMM36 of carbohydrates [36],[37]. Once the molecular model was obtained, a molecular simulation (MD) in vacuum was performed during 2 ns of time to achieve a compact structure. Then, the structure was solvated with TIP3P [38] water with a salt concentration of 0.15 M of NaCl to simulate a physiological environment. MD was performed during 10 ns of time under the isobaric-isothermal ensemble (NPT) using NAMD2.9 software [39].

The molecular model of siRNA (sense: 5'-GUAUAUACAUUCAGCUAAUAU-3', antisense: 5'-AUAUUAGCUGAAUGUAUAUAC-3') was built using the Maestro software [40], employing a double stranded RNA model as a template and later assigned to the CHARMM36 force field for nucleic acids [41]. The structure was minimized using the NAMD 2.11 software [39] (2000 steps). Finally, a molecular dynamics simulation with TIP3P [38] model of water with a concentration of 0.15 M of NaCl was performed during 50 ns of time using NAMD software.

Once obtained the structures of the individual molecules and siRNA in water, both molecules at 44 Å of center-of-mass distance were inserted in a water box (TIP3P), using the same conditions mentioned above, generating six molecular systems. These systems were prepared in the same way as aforementioned, four at neutral pH and two at full protonation state and MD was performed during 50 ns.

All simulations involved in this study were performed using NAMD 2.11. Equations of motion were integrated using a time step of 2 fs using the Verlet algorithm [42]. Langevin dynamics with a damping coefficient of 1 ps and Nosé–Hoover Langevin piston method [43] was applied for maintaining constant temperature and pressure (1 atm). Hydrogen bonds were constrained using RATTLE algorithm [44],[43]. Long-range electrostatic interactions were calculated with Particle mesh Ewald (PME) algorithm [43],[45] and van der Waals forces were estimated using a cutoff of 10 Å. The free energy for each molecular nanoparticle, siRNA and molecular nanoparticle/siRNA nanocomplexe was estimated with MM-GBSA method [43],[46] as follows:

$$G_{TOTAL} = H_{MM} + G_{solv} - T\Delta S_{conf}$$

H_{MM} contribution corresponds to the sum of the terms calculated from MD simulations, specifically from the last 10 ns of each MD trajectory of the molecular nanoparticle, siRNA and molecular nanoparticle/siRNA systems. Solvation free energy G_{solv} was obtained through Generalized Born approach and solvent accessible surface area (SASA). The conformational entropy was not included, because of the large computational cost and low prediction accuracy. Binding free energy was obtained by the difference:

$$\Delta G = G_{TOTAL}\,(\text{nanocomplex}) - G_{TOTAL}\,(\text{molecular NP}) - G_{TOTAL}\,(\text{siRNA})$$

Results

Molecular nanoparticle synthesis

In this work we have considered two structurally related pairs of polycationic amphiphilic cyclooligosaccharides differing in the central carbohydrate platform, namely cyclotrehalans EMA5 and EMA6 and β-cyclodextrin derivatives AMC6 and AMC36. The four compounds feature a polycationic amphiphilic architecture with opposite-oriented polycationic and hydrophobic domains. Their chemical structure was purposely selected to allow exploring the influence of controlled modifications in the cationic heads in their ability to efficiently transfect siRNA. In the two newly synthesized compounds EMA5 and EMA6, the six secondary hydroxyl groups in one of the α,α'-trehalose moieties of the carbohydrate platform are esterified by myristoyl chains and the six hydroxyls in the opposite moiety have been etherified with aminoalkyl antennae (Figure 1). In EMA5, each arm has a single terminal amino group; its preparation involves a macrocyclization reaction of conveniently functionalized trehalose precursors that already incorporate the lipophilic tails and the basic amine functionalities (in protected form), following a convergent approach (see Supporting Information). In EMA 6 the cationic domain has been extended in a dendritic fashion by installing a bis(2-aminoethyl)aminethylthioureido group at the periphery of each of the six branches by multiconjugation of EMA5 with an isothiocyanate-armed partner. The other pair of compounds entails a polycationic amphiphilic β-cyclodextrin scaffold bearing tetra (AMC6) or pentaethylenimine branches (AMC36) at the seven primary positions (Figure 1). The synthesis of AMC6

has been already described and involves a multiple copper(I)-catalyzed azide-alkyne cycloaddidition (CuAAC) “click”-type reaction, leading to the formation of triazol linkers [28]. A parallel strategy was followed to access the homologous compound AMC36. The detailed synthesis and the NMR spectra are collected in the Supporting Information section.

Nanoparticle/siRNA interaction

All four cyclooligosaccharide amphiphiles included in this study have protonable groups and were positively charged at the pH at which the experiments were performed. Accordingly, they were able to bind siRNA at molecular NP/siRNA molar ratios between 5 and 10, corresponding to N/P rations of 4.29 to 6.67 as seen by agarose gel retardation experiments (Figure 3). However, in spite of their overall chemical and structural resemblance, we found striking differences in their capabilities to protect bound siRNA from degradation by RNAses, which is a critical property for a good transfection system. So, whereas both β-cyclodextrin-oligoethyleneimine conjugates AMC6 and AMC36 and the dendritic aminothiourea-armed cyclotrehalan EMA6 impart full protection against RNAse-mediated degradation of their siRNA cargo, the nanocomplexes formulated with the amphiphilic cyclotrehalan derivative EMA5, having six primary amino groups in the cationic heads and lacking the thiourea segments, were unable to protect the siRNA from the RNAses present in the environment and to avoid enzymatic hydrolysis under the same experimental conditions (Figure 4), pointing to important differences in the corresponding molecular interactions at play.

Molecular modelling of NP/siRNA interaction

To evaluate, at the atomic-level, the phenomena behind the striking differences in siRNA protection capabilities against RNAse-mediated degradation between the two polycationic amphiphilic cyclotrehalan-based NPs EMA6, having a thiourea functionality and 18 protonable amino groups at the cationic domain, and EMA5, missing the thiourea group and displaying 6 primary amino groups at its periphery, we decided to perform molecular dynamics simulations that were carried out at full-atomistic scale. The goal was to gain insights in the interactions that are involved in the binding of those macromolecules to siRNA. In a first round, siRNA and NPs were first modeled at a protonation state that simulates physiological pH at which the complexes NP/siRNA are exposed to serum RNAses when added to the cell culture. Dynamics of the interaction between siRNA and EMA5 or EAM6 nanoparticles as a function of time was monitored through the Center of Mass distance to siRNA for both cyclotrehalan derivatives (Figure 5A). This analysis provided us a coarse approach about which molecular NP presents a better interaction with siRNA. EMA6 binds siRNA to a shorter distance than EMA5. To be efficient in protecting its siRNA cargo from RNAse-mediated degradation, the molecular NP needs to minimize the siRNA surface area exposed to solvent and so to RNAse by covering the maximal siRNA surface. When we calculated the solvent accessible surface area (SASA) it became evident that EMA6 covered a larger siRNA surface area than EMA5 (Figure 5B), minimizing siRNA exposure to RNAse as shown in the snapshots of the last frame of MD simulation (Figures 5C-D).

These observations were further complemented when the free energy of binding ($\Delta G_{binding}$) was calculated for each molecular NP/siRNA complex (Table 1), showing that formation of the EMA6/siRNA complex was favored as compared with formation of the EMA5/siRNA complex (i.e. $\Delta G_{binding}$ decreased) by 50.7 kcal/mol. This result is consistent with previous observations pointing to a synergistic effect between hydrogen-bonding and electrostatic interactions in the reversible complexation of oligonucleotides by aminothiourea clusters [47] as well as the superiority of dendritic presentations of the cationic centers over architectures encompassing a single amino group per branch [48]. All these evidences can explain at atomic level why EMA6 protects siRNA from degradation while EMA5 does not.

Transfection efficiency and endosomal escape

siRNA protection from RNAse-mediated degradation is only the first step towards an efficient transfection. Indeed, carriers exhibiting similar protecting abilities may drastically differ in their transfection efficiencies. Thus, while the β-cyclodextrin derivative AMC6 was very efficient at mediating siRNA transfection in several cell lines, the related molecular NP AMC36 did not show any transfection ability (Figure 6). On the other hand, the commercially available transfection agent Interferin® showed a similar transfection efficiency as AMC6. This difference in transfection efficiency between AMC6 and AMC36 was observed for rat C6 glioblastoma cells as well as for other cell lines (human U87 glioblastoma and PC3 prostate cancer cells; data not shown). To exclude that the observed difference in transfection efficiency was due to different abilities to induce endosomal escape, we decided to study the endosome escaping abilities of the nanocomplexes formulated with both molecular

NPs AMC6 and AMC36, using the rat glioblastoma C6 cell line as a suitable biological model. Once the nanocomplex is in the cell interior, release of the siRNA cargo must occur in order to achieve efficient transfection levels. This process is preceded by the escape from the endosomal compartment, which presumably relays on the capability of the vector to cause chloride anion and water entry, osmotic swelling and vacuole disruption, ultimately leading to release of the molecular NPs and their cargo to the cell cytosol [17]. The ability of the nanocomplex formulations to release calcein from endosomal compartments was used as endosomal escape test. When calcein is taken up by cells, it remains in the endosomal compartments and thus a punctuate pattern of fluorescence in the cytoplasm is visible. In the presence of an agent promoting endosomal escape, e. g. the fourth generation poly(amidoamine) cationic dendrimer (PAMAM-G4) with 64 terminal primary amino groups at the periphery, calcein is released into the cytosol yielding a uniform pattern of fluorescence. When a similar assay was conducted in the presence of the β-cyclodextrin-based molecular NPs AMC6 or AMC36, a fluorescence pattern analogous to that obtained with the PAMAM-G4 control was obtained, indicative of similar endosomal escape properties (Figure 7). Although AMC36 showed a slower time-course as compared with AMC6, both compounds showed a similar ability to release calcein from the endosomal compartment [31].The small differences in time-course at this step of the transfection pathway cannot be accountable for the observed drastic differences in overall siRNA transfection (Figure 7). An obvious additional information obtained from the endosomal escape studies is that nanocomplexes formulated with AMC6 or AMC36 are internalized into C6

glioblastoma cells. We thus turned our attention to investigate siRNA dissociation from the nanocomplexes, another critical barrier for efficient transfection that is inversely proportional to the binding energy between the molecular NP and siRNA. If the interaction between the polycationic NPs and siRNA was too strong, this might prevent dissociation of siRNA from the corresponding complex and preclude its biological actions. Getting information on the interactions at play between the cyclooligosaccharide-based NPs and siRNA at acidic pH may thus provide an explanation for the observed experimental differences.

Molecular modelling of molecular NP/siRNA interaction at full protonated state.

In order to emulate the acidic environment at the endosome, the molecular structures for AMC6 and AMC36 in a fully-protonated state, resembling their possible protonation state in endosomes, were built and their interaction with siRNA were modelled *in silico*. Last snapshot of MD simulations of both systems are depicted in Figure 8. The corresponding SASA plots calculations indicated that a single AMC6 NP covered 858 $Å^2$ of the siRNA surface while in the case of AMC36 the covered surface increased up to 1,292 $Å^2$. These results suggest that, at acidic pH resembling the endosome, the presence of the extra ethyleneamino segments in AMC36 as compared to AMC6 translates into a higher number of cationic branches directly interacting with siRNA, leading to stronger binding. Molecular dynamics simulations of the interactions of both β-cyclodextrin-based NPs with siRNA confirmed this hypothesis. Thus, the differences in $\Delta G_{binding}$ values ($\Delta\Delta G_{binding}$) when considering

protonation of the primary amino groups exclusively or of all secondary and primary amino groups were found to increase from 37.8 kcal/mol for AMC6 to 104.7 kcal/mol for AMC36, almost 3-fold higher (Table 2).This implies a much higher stability for the AMC36/siRNA complex as compared to the AMC6/siRNA complex upon cell uptake, therefore a much higher dissociation barrier, which might explain the better performance of AMC6 as transfection reagent.

Discussion

Genetic material, more specifically siRNA, transfection into different cell types represent a new therapeutic option that holds great potential since almost every protein, including some non-druggable proteins involved in the pathogenesis of certain diseases, can be targeted. However, the design of biocompatible and safe carriers enabling siRNA-based therapies constitutes a considerable challenge and represents nowadays the main limitation to this approach. Up to date, there are no clear rules on the characteristics that a chemical system should fulfill to be an efficient transfection agent, which is due to a great extent to the difficulties in accessing molecular prototypes with precise chemical structure, well-suited for conducting structure-activity relationship studies. The only clear requirement for a vector to be able to efficiently transfect siRNA is the presence of positive charges, generally on its surface, to interact with the negatively charged siRNA [49]. After binding, a nanocomplex is formed than must protect siRNA from RNAse-mediated degradation [50] before being taken up by the cell, generally, by an endocytotic mechanism [51]. Once inside the cell, to be efficient, the nanocomplex must escape from the endosome before reaching the lysosome and subsequently release its cargo, allowing siRNA to act on its target mRNA [52].

The recent development of efficient methodologies to access polycationic macromolecules with total control of their chemical structure and purity and with nucleic acid complexation capabilities offer a unique opportunity to get information on the molecular determinants underlining the whole process leading to a successful siRNA transfection. Towards this aim, we have now synthesized two pairs of

multihead-multitail polycationic amphiphilic cyclooligosaccharides based on a cyclotrehalane (EMA5 and EMA6) or a β-cyclodextrin core (AMC6 and AMC36). In spite of having analogous overall chemical architectures, these molecular nanoparticles exhibited striking differences in either protecting siRNA from RNAse-mediated degradation or overall siRNA transfection efficiency, even for pairs sharing the same cyclooligosaccharide core. With this molecular NPs in hand, we have proceeded to: (i) assess their aptitude to complex and deliver siRNA into cells, (ii) explore the influence of chemical modifications at the cationic heads on their properties, and (iii) get insights on the molecular NP-siRNA interactions, at the atomic level, behind efficient siRNA complexation and transfection. For the later goal we have modeled *in silico* the molecular interactions and the related free energy involved in the binding of the NPs to siRNA.

The two amphiphilic cyclotrehalan derivatives EMA5 and EMA6 differ in the number and distribution of cationizable amino groups (6 primary in EMA5; and 12 primary and 6 tertiary in EMA6) and in the absence (EMA5) or presence (EMA6) of a thiourea group per branch (6 in total) in the hydrophilic domain. Both compounds bind efficiently siRNA due to the electrostatic interaction between their positive charges and the negatively charged siRNA. However, in spite of their similar topology, EMA5 is not able to protect its siRNA cargo from degradation by RNAses while EMA 6 affords full protection. The 21 base pairs siRNA has a length of 5.9 nm as measured previously by us using atomic force microscopy [53]. Since the reported persistence length for siRNA is 70 nm [54], several times the measured length for the siRNA used in the present experiments, it can be considered that our siRNA behaves as a

rigid rod. This strongly suggests that the siRNA protecting efficiency of the NPs will be directly related to the ability to cover the siRNA rod surface, preventing the access of RNAses. We explored this hypothesis by *in silico* modeling the binding process. The data indicated that a single EMA5 molecular NP covered 418 $Å^2$ of the siRNA surface while in the case of EMA6 the covered surface almost doubled (818 $Å^2$), limiting the access of RNAses to siRNA. It can be reasonably assumed that a better performance of a single molecular NP at covering siRNA surface translates into a more compact encapsulation of siRNA in the corresponding nanocomplexes, which is likely at the origin of observed differences in siRNA protection capabilities. More interestingly, these results support that the solvent accessible surface area value for siRNA bound to a given molecular NP can be considered a good predictor for its ability to protect siRNA from degradation by RNAses: low and high SASA values correlate with strong and weak siRNA protecting abilities, respectively.

Differently from that observed for the cationic cyclotrehalan pair, the polycationic amphiphilic β-cyclodextrin derivative AMC6 [28] and the newly synthesized homologue molecule AMC36, having an extra ethyleneimine segment in each of the seven branches that form the polycationic domain, were both able to fully protect siRNA from degradation by RNAse after formulation of the corresponding nanocomplexes. However, whereas AMC6 mediated transfection of siRNA into glioma C6 and other cell lines, decreasing the levels of the target protein to about 70% of control values at 72 hours after transfection, meaning an efficiency very similar to that of the commercial product Interferin® used as reference, AMC36 was unable to produce any siRNA transfection. No significant differences were observed

for both nanoparticles in terms of promoting endosomal escape, beyond a slight delay for nanocomplexes formulated with AMC36 as compared with AMC6, suggesting that the origin of the differences in transfection efficiency is at a farther step. This led to us to explore the effect of the structural differences existing between AMC6 and AMC36 on the ability of the corresponding molecular NP/siRNA nanocomplexes to dissociate and free the siRNA payload, which can then bind the target mRNA and induce its degradation [55].

Molecular dynamics simulations indicated that the $\Delta G_{binding}$ values for molecular NP/siRNA complex formation become more negative (the stability increases) when considering a fully-protonated state of AMC6 or AMC36 as compared to protonation at the primary amino groups only. The degree of stabilization of the nanocomplexes after full protonation was, however, very different for each vector: $\Delta G_{binding}$ of AMC36 increased in 104.7 kcal/mol upon full protonation while in the case of AMC6 only grew in 37 kcal/mol, indicating that the stability enhancement is almost 3-fold greater for AMC36 as compared with AMC6 (Table 2). This difference might explain the better performance of AMC6 as transfection vector. Indeed, it has been pointed out the importance of designing nucleic acid carriers that allow transporting and protecting nucleic acids and that, at the same time, permit the cargo release [56]. A carrier with very high affinity for nucleic acids at full protonation state would not permit the release of nucleic acids, failing in the task of efficiently transfecting cells. In brief, an adequate balance of the binding energy must be achieved between that required to keep the complex assembled in biological fluids and the limit to allow the dissociation of the complex in the proper cellular environment to allow siRNA to

perform its knocking down function [56]. SASA plots obtained from the computational analysis are in agreement with the difference encountered in $\Delta G_{binding}$ for AMC6/siRNA and AMC36/siRNA complexes in the fully protonated state. Thus, while AMC6 affords similar levels of siRNA surface coverage independently of having only the primary or both primary and secondary amine groups protonated, AMC36 shows a reduction in SASA level at full protonated state, strongly suggesting that the extra ethyleneammonium groups in the later establish additional contacts with the siRNA molecule, increasing the affinity of the compound for the nucleic acid and the stability of the resulting nanocomplex. This will make difficult for the siRNA to dissociate, precluding an efficient transfection.

Conclusions

In summary, in this work, we have used a combination of directed chemical synthesis, biological experiments and *in silico* modelling to identify some of the key properties that a non-viral vector should fulfill to perform efficiently as a siRNA transfection agent and correlate subtle structural differences with siRNA protection and transfection capabilities. We have found that the presence of a polycationic domain in amphiphilic cyclooligosaccaride-based molecular nanoparticles, required to bind the negatively charged siRNA, does not warrant efficient protection of the nucleic acid cargo in the corresponding nanocomplexes. The capacity of the non-viral vector to cover the siRNA surface after the initial electrostatic interaction is critical at this regard: a reduced SASA level in the siRNA leads to a higher probability of resistance to RNAse-mediated degradation. Moreover, the increase in the observed molecular NP/siRNA binding energy on going from a partial to a fully protonated state of the vector, should be kept as low as possible to allow the mechanisms leading to siRNA release (e.g., electrostatic repulsions between polycationic clusters in the nanocomplexes, siRNA complexation with negatively charged cytosolic molecules, etc,) to operate. It is important to highlight that, although we have focus in this work on cyclooligosaccharide-type molecular nanoparticles, the *in silico* modeling approach here implemented has a general covation: by predicting both SASA and $\Delta G_{binding}$ for single molecule NP/siRNA interactions, it can provide very valuable hints on the potential as siRNA transfection system of a given molecular vector prototype *a priori*, before it is synthesized; it is therefore well suited for computer-assisted design strategies.

Executive Summary

Molecular nanoparticle synthesis.

- Two structurally related pairs of polycationic amphiphilic cyclo-oligosaccharides differing in the central carbohydrate platform, namely cyclotrehalans EMA5 and EMA6 and β-cyclodextrin derivatives AMC6 and AMC36 have been synthesized.

Molecular nanoparticle/siRNA interaction.

- All four compounds were able to bind siRNA at molecular NP/siRNA molar ratios between 5 and 10, corresponding to N/P rations of 4.29 to 6.67.
- Both β-cyclodextrin derivatives and the cyclotrehalan EMA6 fully protected siRNA from RNAse-mediated degradation. However, the cyclotrehalan EMA5 was not able to protect it.

Molecular modelling of molecular NP/siRNA interactions.

- Molecular modelling, at the atomic level, showed that EMA6 covered a larger siRNA surface area than EMA5, minimizing siRNA exposure to RNAse.
- Accordingly, free energy binding calculations indicated that formation of the EMA6/siRNA complex was favored as compared with formation of the EMA5/siRNA complex.

Transfection efficiency and endosomal escape

- The β-cyclodextrin derivative AMC6 very efficiently mediated siRNA transfection in tumoral cell lines while the closely related molecule, AMC36 did not show any transfection ability.
- Both AMC6 and AMC36 showed similar ability to induce endosomal escape, suggesting that the origin of the differences in transfection efficiency should be placed at a further step.

Molecular modelling of molecular NP/siRNA interaction at full protonated state.

- At full protonated state, AMC36 covered much more siRNA surface than AMC6.
- Free energy binding studies showed that molecular NP/siRNA nanocomplexes were much more stable for AMC36 than for AMC6 formulations, indicating that siRNA dissociation, therefore expression of its biological function, would be favored in the later case.

Summary points

✓ A combination of directed chemical synthesis, biological experiments and *in silico* modelling has been used to identify some of the key molecular determinants for efficient siRNA transfection by a cyclooligosaccharide-based non-viral vector.

✓ Two closely related amphiphilic cyclotrehalan derivatives, EMA5 and EMA6, were synthesized and showed striking differences in siRNA protection capabilities towards degradation by RNAses.

✓ EMA6 fully protects siRNA against RNAse-mediated degradation while EMA5 does not.

✓ Molecular modelling of the molecular NP/siRNA interactions indicates that the siRNA solvent accessible surface area is significantly smaller in the presence of EMA6 as compared with EMA5.

✓ The smaller solvent accessible surface area translates into a more efficient covering of the siRNA in the corresponding nanocomplexes and, consequently, a lower accessibility to RNAses for EMA6 as compared with EMA5 formulations.

✓ Two very closely related amphiphilic β-cyclodextrin derivatives, AMC6 and AMC36, were also synthesized and showed very different transfection efficiency for siRNA targeting p42-MAPK in tumoral cells lines.

✓ AMC6-siRNA complexes reduced p42-MAPK protein levels to about 25% of control values at 72 hours while AMC36-siRNA complexes did not cause any reduction in p42-MAPK protein levels

- ✓ No differences were found between nancomplexes formulated with AMC6 or AMC36 regarding their ability to induce endosomal escape, excluding this as a possible cause of the observed differences in transfection efficiency
- ✓ Molecular modelling studies indicated that AMC36/siRNA complexes were much more stable than AMC6/siRNA complexes under conditions simulating full protonation state of the vectors, suggesting that dissociation and release of the siRNA cargo would be significantly hampered in the first case, precluding its biological action.

Financial disclosure/Acknowledgements

This work was supported by the Spanish Ministerio de Economía y Competitividad (MINECO, grants no. BFU2014-59009-P, SAF2016-76083-R and CTQ2015-64425-C2-1-R), CYTED (grant no. 214RT0482); Fraunhofer Chile Research, Innova Chile CORFO (FCR-CSB 09CEII-6991), the Junta de Andalucía (grant no. FQM2012-1467), the European Union (FEDER and FSE) and the CSIC. The excellent technical work of Ana B. García and Elena Galera as well as the technical assistance by the services of the University of Sevilla (CITIUS) are also acknowledged.

Table 1. Binding energy (Kcal/mol) of cyclotrehalan-based molecular nanoparticle/siRNA complexes obtained from MM/GBSA simulations at neutral pH and the area ($Å^2$) of siRNA covered by each nanoparticle.

	ΔG Complex Kcal/mol	**ΔG NP Kcal/mol**	**ΔG siRNA Kcal/mol**	**$\Delta G_{Binding}$ Kcal/mol**	**$\Delta\Delta G_{Binding}$[a] Kcal/mol**	**siRNA Covered Area $Å^2$**
EMA5	-2,446.8	96.4	-2,518.3	-24.9	50.7	420
EMA6	-2,741.1	-147.2	-2,518.3	-75.6	0	818

[a]$\Delta\Delta G_{Binding}$ is defined as the difference between the $\Delta G_{Binding}$ of both complexes using as reference $\Delta G_{Binding}$ for EMA6.

Table 2. Binding energy (Kcal/mol) of β-cyclodextrin-based molecular nanoparticle/siRNA complexes. Relative free energy of binding obtained from MM/GBSA simulations at physiological and acidic pH.

	ΔG Complex Kcal/mol	**ΔG NP Kcal/mol**	**ΔG siRNA Kcal/mol**	**$\Delta G_{Binding}$ Kcal/mol**	**$\Delta\Delta G_{Binding}$[a] Kcal/mol**
AMC6 physiological pH	-1,961.3	578.9	-2,518.3	-21.9	0
AMC36 physiological pH	-1,913.3	625.5	-2,518.3	-20.5	0
AMC6 acidic pH	-2,365.4	212.6	-2,518.3	-59.7	-37.8
AMC36 acidic pH	-2,438.2	205.3	-2,518.3	-125.2	-104.7

[a]$\Delta\Delta G_{Binding}$ is defined as the difference between the $\Delta G_{Binding}$ at physiological and acidid pH for every complex.

Figure legends

Figure 1. Structures of the polycationic amphiphilic cyclooligosaccharides included in this study. Compounds EMA5 and EMA6 share a cyclotrehalan core, whereas compounds AMC6 and AMC36 are built on a β-cyclodextrin scaffold and differ only in one amino group in every olioethylenimine branch. All compounds are depicted in their fully protonated state.

Figure 2. Fractionation of nanoparticles in molecular blocks for molecular dynamics analysis. Monomers of cyclotrehalans EMA5 and EMA6 (top panel) and β-cyclodextrin derivatives AMC6 and AMC36 nanoparticles (bottom panel) were divided in 3 molecular blocks: TAI blocks correspond to the aliphatic tails of the nanoparticles, COR is the cyclooligosaccharide core that forms a macroring structure, and the cationic heads of the nanoparticles are located in TER blocks.

Figure 3. Gel retardation assay. siRNA (100 nM) was incubated at increasing N/P ratios, indicated at the top of each panel, for 30 min . The reaction mixture was loaded onto a 1.2 % agarose gel and run as indicated in Material and Methods. Figure shows an experiment repeated twice with similar results. Panels represent the data for A) AMC6, B) AMC36; C) EMA5 and D) EMA6 nanoparticles.

Figure 4. RNAse protection. siRNA protection by the different nanoparticles form RNAse-mediated degradation was performed as indicated in Material and Methods. Total amount of recovered intact siRNA was determined by densitometric analysis

and quantified using the Image J program. Data represent mean ± s.e.m. of 3 experiments.

Figure 5: Molecular modeling of the cyclotrahalan-based molecular nanoparticle/siRNA complexes at partially protonated state. Molecular analysis of nanoparticle/siRNA 1:1 complexes considering only protonation of the primary amino groups exclusively. A) Comparison of the distance between the Center Of Mass (COM) of siRNA and cyclotrehalans EMA5 and EMA6 through 50 ns of MD trajectory. B) Solvent accessible surface area (SASA) of siRNA in of the corresponding with EMA5 and EMA6 as a function of time. The main SASA of siRNA in the absence of the cyclotrehalans is represented in black dotted line. Snapshots of the 1:1 complexes formed between EMA5 (C) or EMA6 (D) and siRNA at 50 ns of MD trajectory, are also shown. Cyan sticks represent the cyclotrehalan molecule and siRNA is represented by red double helix.

Figure 6. AMC6 and AMC36-mediated siRNA transfection. AMC6 (A) and AMC36 (B) nanoparticles were used as vehicles to transfect siRNA. Glioblastoma C6 cells were treated for 72 hours with vehicle (Control); 1 µM nanoparticle; complexes formed by 1 µM Nanoparticle/100 nM siRNA against p42-MAPK mRNA; complexes formed by 2 µL Interferin/100 nM siRNA against p42-MAPK mRNA (INT+p42) and complexes formed by 1 µM nanoparticle/100 nM scramble siRNA. Cells were lysed and the content of p42-MAPK relative to β-actin analyzed as indicated in Methods. Data represent mean ± s.e.m. of 4 experiments for AMC6 and 3 for AMC36.

Figure 7. Endosomal escape for the different nanocomplexes. Rat glioblastoma C6 cells were incubated for 4 hours in the presence of calcein (250 μM) alone or together with the different nanoparticles (1 μM) as indicated in Material and Methods. Images were taken at 10 (Control; PAMAM G4 and AMC6) or 12 (AMC36) hours after the beginning of the experiment. No differences for control cells were observed between 10 and 12 hours. Ten minutes before recording, cells were incubated with Hoescht 33342 (25 μg/mL). Cells were then washed using K-H solution and fluorescence determined as indicated in Methods. The panel shows representative images for individual calcein and Hoescht 33342 fluorescence, the overlay of both of them and Nomarski (DIC).

Figure 8. Interaction of fully protonated β-cyclodextrin-based molecular nanoparticles with siRNA. Snapshots of 1:1 complexes of fully protonated AMC6 (C) or AMC36 (D) and siRNA at 50 ns of MD trajectory are shown. Cyan sticks represent the molecular nanoparticles and siRNA is represented by red double helix.

References

1. Sahay G, Querbes W, Alabi C *et al:* Efficiency of siRNA delivery by lipid nanoparticles is limited by endocytic recycling. *Nat.Biotechnol.* 31(7), 653-658 (2013).

2. Posadas I, Perez-Martinez FC, Guerra J, Sánchez-Verdu P, Ceña V: Cofilin activation mediates Bax translocation to mitochondria during excitotoxic neuronal death. *J.Neurochem.* 120(4), 515-527 (2012).

3. Barata P, Sood AK, Hong DS: RNA-targeted therapeutics in cancer clinical trials: Current status and future directions. *Cancer Treat.Rev.* 50, 35-47 (2016).

4. Monteagudo S, Perez-Martinez FC, Pérez-Carrión MD *et al:* Inhibition of p42 MAPK using a nonviral vector-delivered siRNA potentiates the anti-tumor effect of metformin in prostate cancer cells. *Nanomedicine (Lond)* 7(4), 493-506 (2012).

5. Svobodova E, Kubikova J, Svoboda P: Production of small RNAs by mammalian Dicer. *Pflugers Arch.* 468(6), 1089-1102 (2016).

6. Guo J, Jiang X, Gui S: RNA interference-based nanosystems for inflammatory bowel disease therapy. *Int.J.Nanomedicine* 11, 5287-5310 (2016).

7. Catalanotto C, Cogoni C, Zardo G: MicroRNA in Control of Gene Expression: An Overview of Nuclear Functions. *Int.J.Mol.Sci.* 17(10) E1712 (2016).

8. Curtis CD , Nardulli AM: Using RNA interference to study protein function. *Methods Mol.Biol.* 505, 187-204 (2009).

9. Janiszewska J, Posadas I, Játiva P, Bugaj-Zarebska M, Urbanczyk-Lipkowska Z, Ceña V: Second Generation Amphiphilic Poly-Lysine Dendrons Inhibit Glioblastoma Cell Proliferation without Toxicity for Neurons or Astrocytes. *PLoS One* 11(11), e0165704- (2016).

10. Pérez-Carrión MD, Perez-Martinez FC, Merino S *et al:* Dendrimer-mediated siRNA delivery knocks down Beclin 1 and potentiates NMDA-mediated toxicity in rat cortical neurons. *J.Neurochem.* 120(2), 259-268 (2012).

11. Aigner A , Fischer D: Nanoparticle-mediated delivery of small RNA molecules in tumor therapy. *Pharmazie* 71(1), 27-34 (2016).

12. Inoue Y, Kurihara R, Tsuchida A *et al:* Efficient delivery of siRNA using dendritic poly(L-lysine) for loss-of-function analysis. *J.Control Release* 126(1), 59-66 (2008).

13. Perez AP, Cosaka ML, Romero EL, Morilla MJ: Uptake and intracellular traffic of siRNA dendriplexes in glioblastoma cells and macrophages. *Int.J.Nanomedicine.* 6, 2715-2728 (2011).

14. Goldshtein M, Forti E, Ruvinov E, Cohen S: Mechanisms of cellular uptake and endosomal escape of calcium-siRNA nanocomplexes. *Int.J.Pharm.* 515(1-2), 46-56 (2016).

15. Sarisozen C, Salzano G, Torchilin VP: Lipid-based siRNA Delivery Systems: Challenges, Promises and Solutions Along the Long Journey. *Curr.Pharm.Biotechnol.* 17(8), 728-740 (2016).

16. Liu X, Liu C, Zhou J *et al:* Promoting siRNA delivery via enhanced cellular uptake using an arginine-decorated amphiphilic dendrimer. *Nanoscale* 7(9), 3867-3875 (2015).

17. Boussif O, Lezoualc'h F, Zanta MA *et al:* A versatile vector for gene and oligonucleotide transfer into cells in culture and in vivo: polyethylenimine. *Proc.Natl.Acad.Sci.U.S.A* 92(16), 7297-7301 (1995).

18. Ortiz Mellet C, Benito JM, Garcia Fernandez JM: Preorganized macromolecular gene delivery systems. *Chem.Eur.J.* 16, 6728-6742 (2010).

19. Gallego-Yerga L, Lomazzi M, Franceschi V *et al:* Cyclodextrin- and calixarene-based polycationic amphiphiles as gene delivery systems: a structure-activity relationship study. *Org.Biomol.Chem.* 13, 1708-1723 (2015).

20. Pflueger I, Charrat C, Ortiz Mellet C, Garcia Fernandez JM, Benito JM: Cyclodextrin-based facial amphiphiles: assessing the impact of the hydrophilic–lipophilic balance in the self-assembly, DNA complexation and gene delivery capabilities. *Org.Biomol.Chem.* 14, 10037-10047 (2016).

21. Jimenez Blanco JL, Ortega-Caballero F, Blanco-Fernandez L *et al:* Trehalose-based Janus cyclooligosaccharides: the "click" synthesis and DNA-

directed assembly into pH-sensitive transfectious nanoparticles. *Chem Commun (Camb)* 52, 10117-10120 (2016).

22. Ortiz Mellet C, García Fernández JM, Benito JM: Cyclodextrin-based gene delivery systems. *Chem Soc Rev* 40, 1586-1606 (2011).

23. Mendez-Ardoy A, Gomez-Garcia M, Ortiz Mellet C *et al:* Preorganized macromolecular gene delivery systems: amphiphilic beta-cyclodextrin "click clusters". *Org.Biomol.Chem.* 7(13), 2681-2684 (2009).

24. Srinivasachari S, Fichter KM, Reineke TM: Polycationic beta-cyclodextrin "click clusters": monodisperse and versatile scaffolds for nucleic acid delivery. *J.Am.Chem Soc* 130(14), 4618-4627 (2008).

25. Garcia Fernandez JM, Ortiz Mellet C, Jimenez Blanco JL *et al:* Isothiocyanates and cyclic thiocarbamates of alpha,alpha'-trehalose, sucrose, and cyclomaltooligosaccharides. *Carbohydr.Res.* 268(1), 57-71 (1995).

26. Jimenez Blanco JL, Ortega-Caballero F, Blanco-Fernández L *et al:* Trehalose-based Janus cyclooligosaccharides: the "Click" synthesis and DNA-directed assembly into pH-sensitive transfectious nanoparticles. *Chem.Commun.(Camb.)* 52(66), 10117-10120 (2016).

27. Diaz-Moscoso A, Le Gourrierec L, Gómez-García M *et al:* Polycationic amphiphilic cyclodextrins for gene delivery: syntehsis and effect of structural modifications on plasmid DNA complex stability, citotoxicity

and gene expression. *Chemistry - A European Journal* 15(46), 12871-12888 (2009).

28. Martinez A, Bienvenu C, García-Fernández JM, Jiménez JL, DiGiorgio C: Amphiphilic Oligoethyleneimine-ß-Cyclodextrin "Click" Clusters for Enhanced DNA Delivery. *Journal of Organic Chemistry* 78, 8143-8148 (2013).

29. Rodrigo AC, Rivilla I, Perez-Martinez FC *et al:* Efficient, Non-Toxic Hybrid PPV-PAMAM Dendrimer as a Gene Carrier for Neuronal Cells. *Biomacromolecules.* 12(4), 1205-1213 (2011).

30. Schindelin J, Arganda-Carreras I, Frise E *et al:* Fiji: an open-source platform for biological-image analysis. *Nat.Methods* 9(7), 676-682 (2012).

31. Veiseh O, Kievit FM, Fang C *et al:* Chlorotoxin bound magnetic nanovector tailored for cancer cell targeting, imaging, and siRNA delivery. *Biomaterials* 31(31), 8032-8042 (2010).

32. Perez-Carrion MD , Ceña V: Knocking down HMGB1 using dendrimer-delivered siRNA unveils its key role in NMDA-induced autophagy in rat cortical neurons. *Pharm.Res.* 30(10), 2584-2595 (2013).

33. Márquez-Miranda V, Camarada MB, Araya-Durán I, Varas-Concha I, Almonacid DE, González-Nilo FD: Biomimetics: From Bioinformatics to Rational Design of Dendrimers as Gene Carriers. *PLoS One* 10, e0138392 (2015).

34. Vanommeslaeghe K, Hatcher E, Acharya C *et al:* CHARMM general force field: A force field for drug-like molecules compatible with the CHARMM all-atom additive biological force fields. *J.Comput.Chem.* 31, 671-690 (2010).

35. Vanommeslaeghe K , Mackerell AD: Automation of the CHARMM General Force Field (CGenFF) I: bond perception and atom typing. *J Chem Inf Model* 52, 3144-3154 (2012).

36. Raman EP, Guvench O, MacKerell AD: CHARMM Additive All-Atom Force Field for Glycosidic Linkages in Carbohydrates Involving Furanoses. *J.Phys.Chem.B* 114, 12981–12994 (2010).

37. Guvench O, Mallajosyula SS, Raman EP *et al:* CHARMM Additive All-Atom Force Field for Carbohydrate Derivatives and Its Utility in Polysaccharide and Carbohydrate–Protein Modeling. *Journal of Chemical Theory and Computation* 7, 3162–3180 (2011).

38. Jorgensen WL, Chandrasekhar J, Madura JD, Impey RW, Klein ML: Comparison of simple potential functions for simulating liquid water. *The Journal of Chemical Physics* 79(2), 926-935 (1983).

39. Phillips JC, Braun R, Wang W *et al:* Scalable molecular dynamics with NAMD. *J.Comput.Chem.* 26, 1781-1802 (2005).

40. Maestro version 10.4.018, Schrödinger, LCC, New York, NY, (2015).

41. Denning EJ, Priyakumar UD, Nilsson L, MacKerell AD: Impact of 2'-hydroxyl sampling on the conformational properties of RNA: Update of the CHARMM all-atom additive force field for RNA. *J.Comput.Chem.* 32, 1929-1943 (2011).

42. Tuckerman M, Berne BJ, Martyna GJ: Reversible multiple time scale molecular dynamics. *The Journal of Chemical Physics* 97, 1990-2001 (1992).

43. Martyna GJ, Tobias DJ, Klein ML: Constant pressure molecular dynamics algorithms. *The Journal of Chemical Physics* 101, 4177-4189 (1994).

44. Andersen HC: Rattle: A “velocity” version of the shake algorithm for molecular dynamics calculations. *Journal of Computational Physics* 52, 24-34 (1983).

45. Essmann U, Perera L, Berkowitz ML, Darden T, Lee H, Pedersen LG: A smooth particle mesh Ewald method. *The Journal of Chemical Physics* 103, 8577-8593 (1995).

46. Gohlke H , Case DA: Converging free energy estimates: MM-PB(GB)SA studies on the protein-protein complex Ras-Raf. *J.Comput.Chem.* 25, 238-250 (2004).

47. Méndez-Ardoy A, Guilloteau C, DiGiorgio P *et al:* b-Cyclodextrin-based polycationic amphiphilic "click" clusters: Effect of structural modifications in their DNA complexing and delivery properties. *J.Org.Chem.* 76(15), 5882-5894 (2011).

48. Gallego-Yerga L, González-Alvárez MJ, Mayordomo N *et al:* Dynamic self-assembly of polycationic clusters based on cyclodextrins for pH-sensitive DNA nanocondensation and delivery by component design. *Chemistry* 20(22), 6622-6627 (2014).

49. Israel LL, Lellouche E, Ostrovsky S *et al:* Acute in vivo toxicity mitigation of PEI-coated maghemite nanoparticles using controlled oxidation and surface modifications toward siRNA delivery. *ACS Appl.Mater.Interfaces.* 7(28), 15240-15255 (2015).

50. Cohen ZR, Ramishetti S, Peshes-Yaloz N *et al:* Localized RNAi therapeutics of chemoresistant grade IV glioma using hyaluronan-grafted lipid-based nanoparticles. *ACS Nano* 9(2), 1581-1591 (2015).

51. Majzoub RN, Wonder E, Ewert KK, Kotamraju VR, Teesalu T, Safinya CR: Rab11 and Lysotracker Markers Reveal Correlation between Endosomal Pathways and Transfection Efficiency of Surface-Functionalized Cationic Liposome-DNA Nanoparticles. *J.Phys.Chem.B* 120(26), 6439-6453 (2016).

52. Ahmad A, Ranjan S, Zhang W, Zou J, Pyykko I, Kinnunen PK: Novel endosomolytic peptides for enhancing gene delivery in nanoparticles. *Biochim.Biophys.Acta* 1848(2), 544-553 (2015).

53. Dumitru AC, Herruzo ET, Rausell E, Ceña V, García R: Unbinding forces and energies between a siRNA molecule and a dendrimer measured by force spectroscopy. *Nanoscale* 7(47), 20267-20276 (2015).

54. Abels JA, Moreno-Herrero F, van der Heijden T, Dekker C, Dekker NH: Single-molecule measurements of the persistence length of double-stranded RNA. *Biophys.J.* 88(4), 2737-2744 (2005).

55. Roberts TC, Ezzat K, El AS, Weinberg MS: Synthetic SiRNA Delivery: Progress and Prospects. *Methods Mol.Biol.* 1364, 291-310 (2016).

56. Pavan GM, Monteagudo S, Guerra J *et al:* Role of Generation, Architecture, pH and Ionic Strength on Successful siRNA Delivery and Transfection by Hybrid PPV-PAMAM Dendrimers. *Curr.Med.Chem.* 19(29), 4929-4941 (2012).

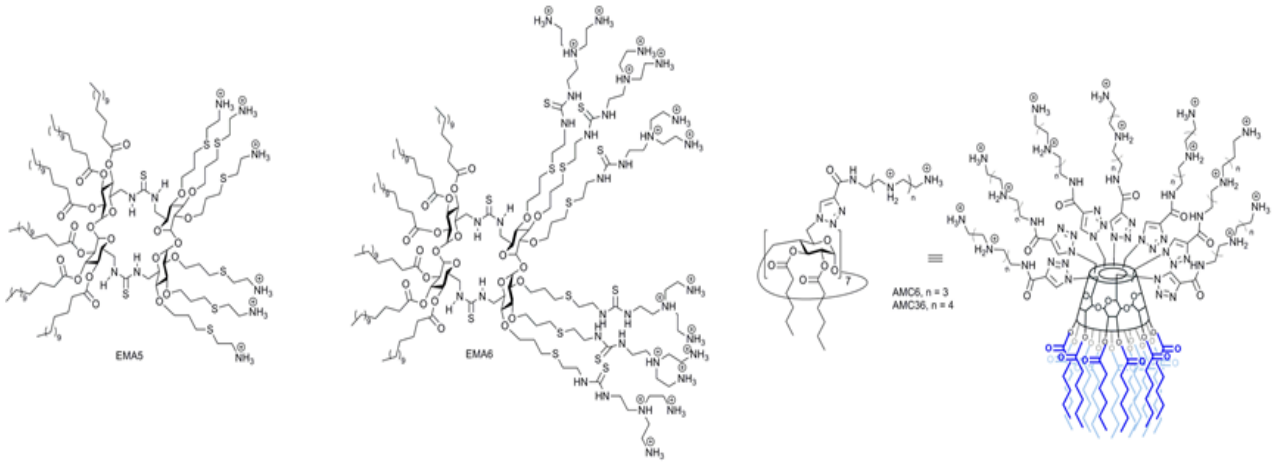

Figure 1

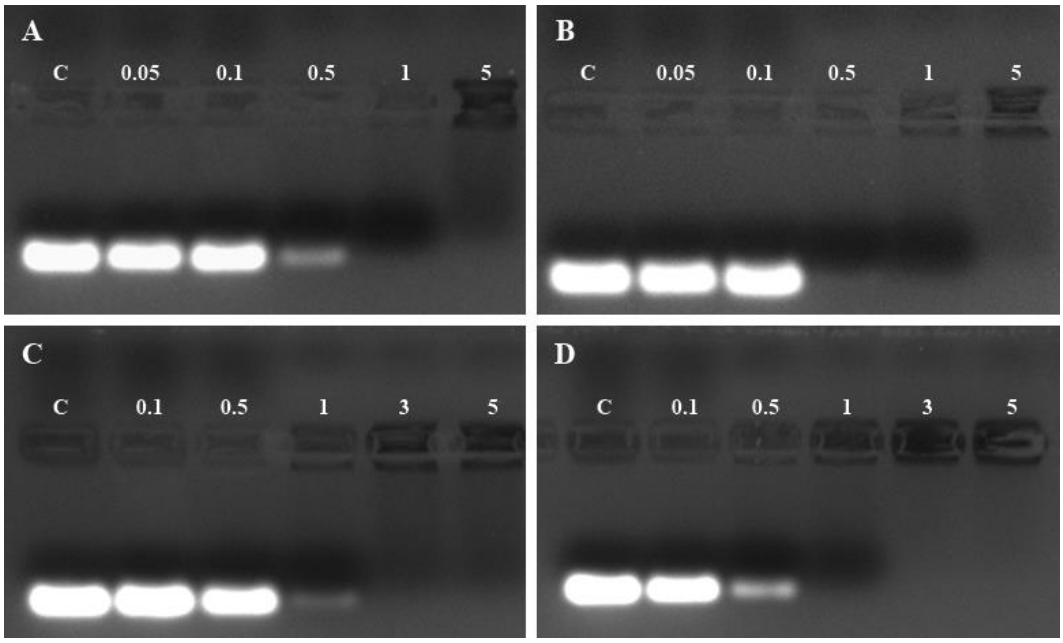

Figure 2

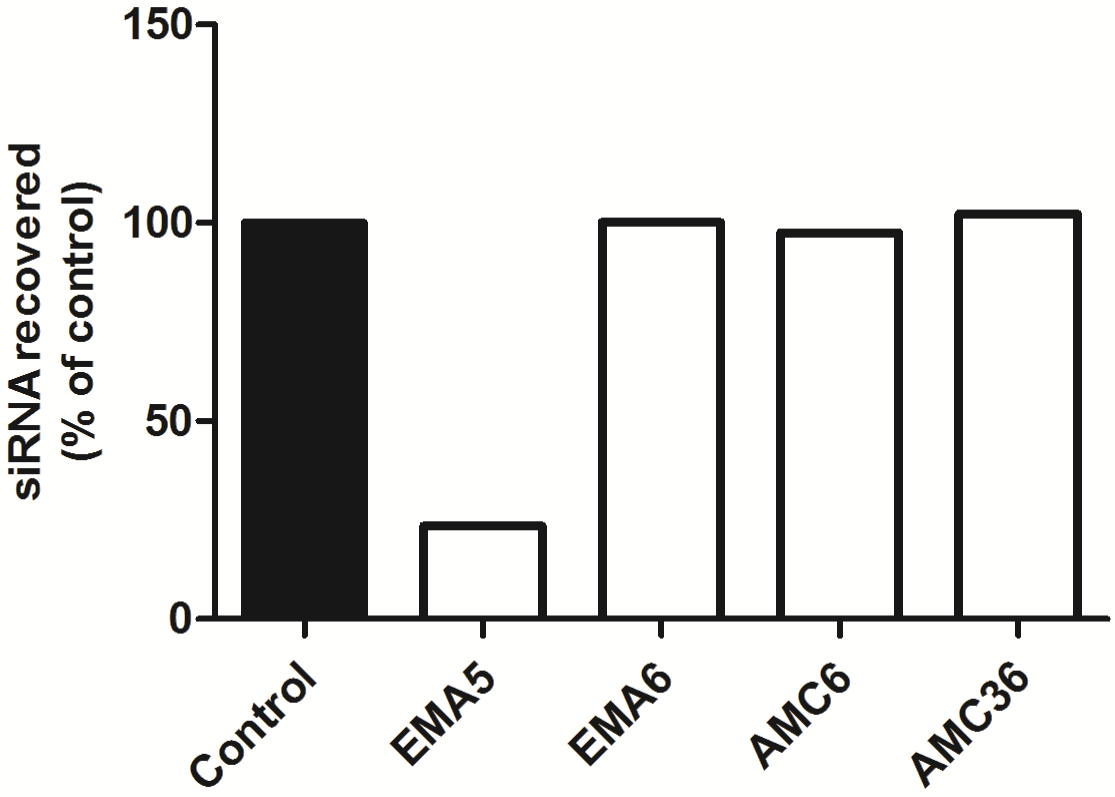
150
100
50
0
siRNA recovered
(% of control)
Control
EMA5
EMA6
AMC6
AMC36

Figure 3

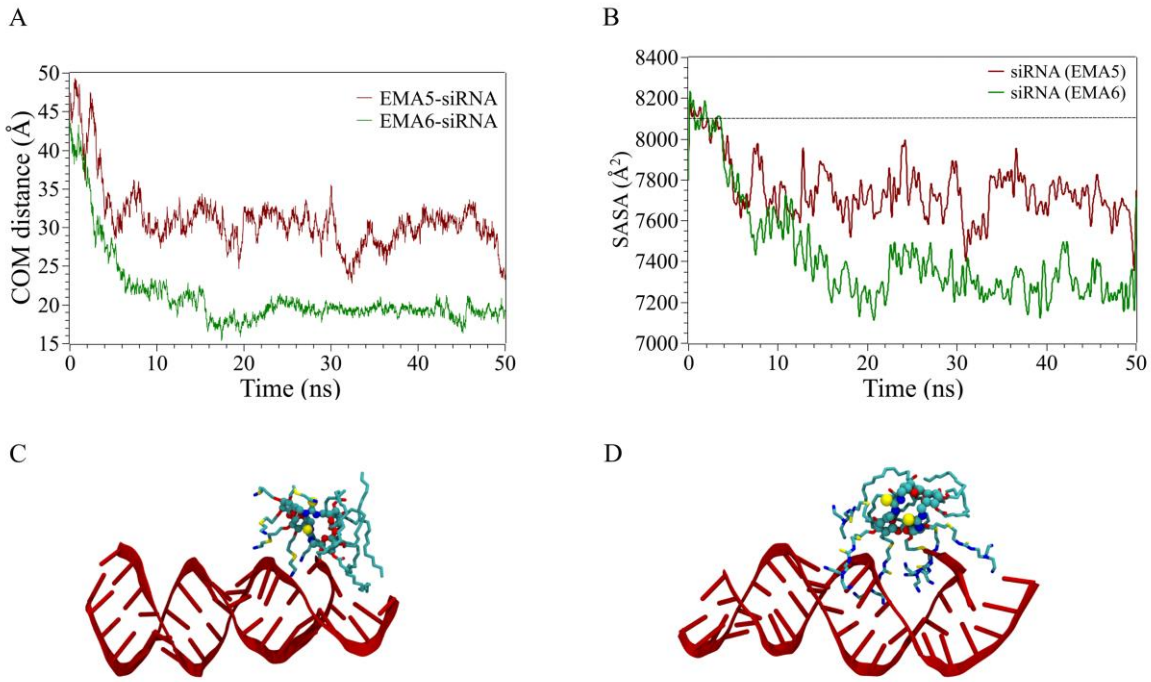
A
B
EMA5-siRNA
EMA6-siRNA
COM distance (Å)
Time (ns)
siRNA (EMA5)
siRNA (EMA6)
SASA (Å²)
Time (ns)
C
D

Figure 4

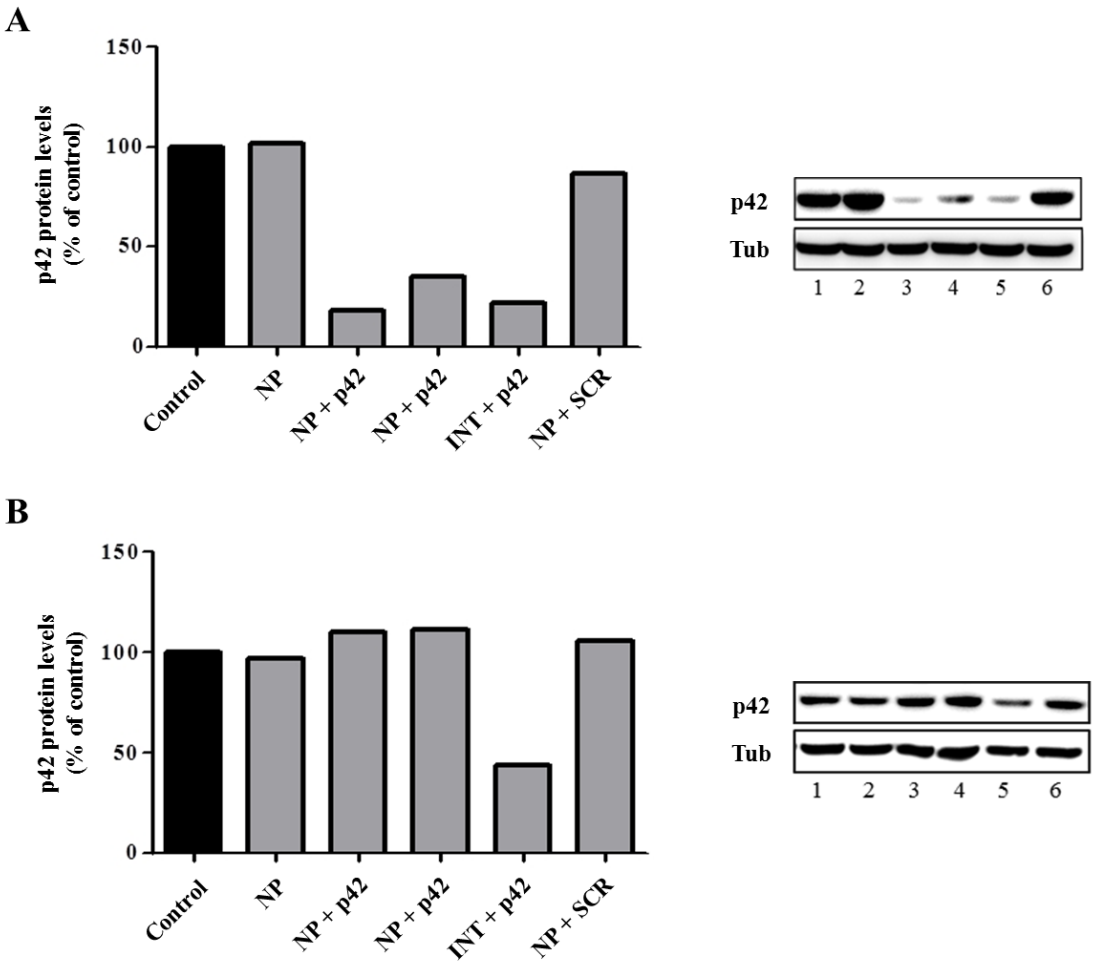
A
150
100
50
0
p42 protein levels
(% of control)
Control
NP
NP + p42
NP + p42
INT + p42
NP + SCR
p42
Tub
1 2 3 4 5 6
B
150
100
50
0
p42 protein levels
(% of control)
Control
NP
NP + p42
NP + p42
INT + p42
NP + SCR
p42
Tub
1 2 3 4 5 6

Figure 5

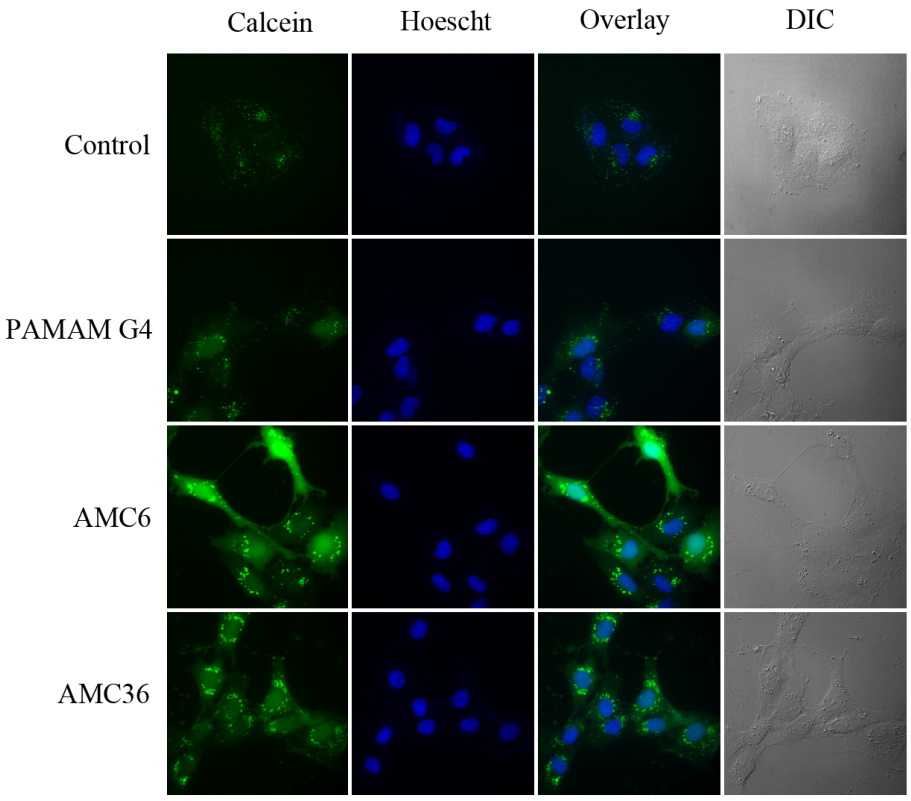

Figure 6

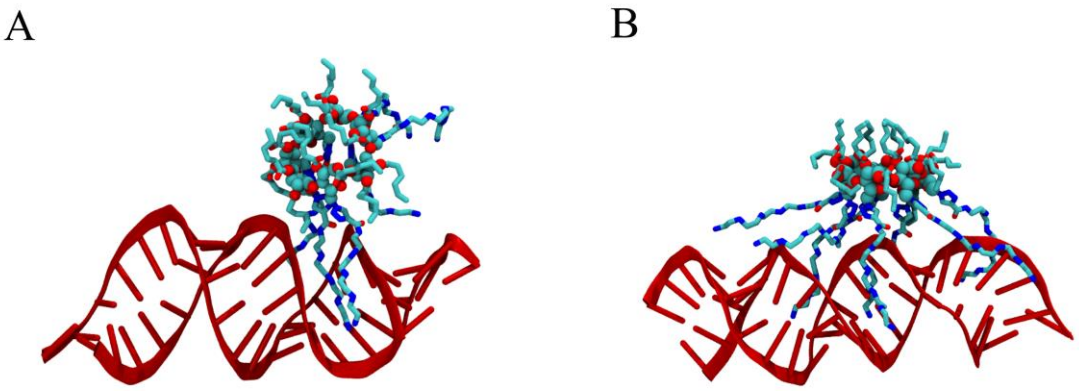

Figure 7

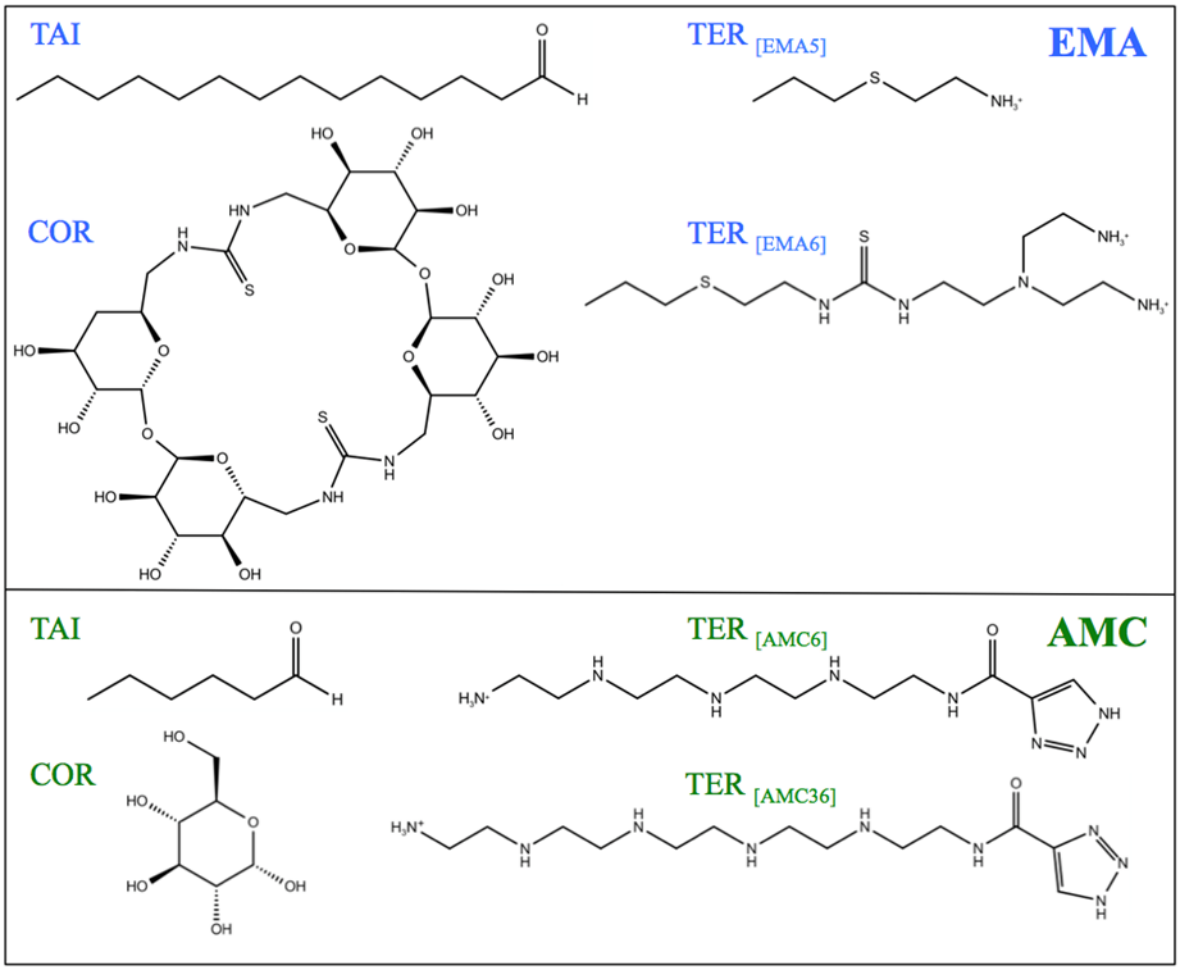

Figure 8